Defect-free outer-selective hollow fiber thin-film composite membranes for forward osmosis applications

Sungil Lim, Van Huy Tran, Nawshad Akther, Sherub Phuntsho and Ho Kyong Shon*

Centre for Technology in Water and Wastewater (CTWW), School of Civil and Environmental Engineering, University of Technology Sydney (UTS), Australia

* Corresponding author: Prof. Ho Kyong Shon Email: hokyong.shon-1@uts.edu.au; Tel.: +61 2 9514 2629; Fax: +61 2 9514 2633.

Keywords: Outer-selective; Thin-film composite; Hollow fiber; Forward osmosis; Vacuum-assisted Interfacial polymerization.

Abstract

This study presents the successful fabrication of a novel defect-free outer-selective hollow fiber (OSHF) thin-film composite (TFC) membrane for forward osmosis (FO) applications. Thin and porous FO membrane substrates made of polyether sulfone (PES) with a dense and smooth outer surface were initially fabricated at different air-gap distances. A modified vacuum-assisted interfacial polymerisation (VAIP) technique was then successfully utilised for coating polyamide (PA) layer on the hollow fiber (HF) membrane substrate to prepare OSHF TFC membranes. Experimental results showed that the molecular weight cut-off (MWCO) of the surface of the membrane substrate should be less than 88 kDa with smooth surface roughness to obtain a defect-free PA layer via VAIP. The FO test results showed that the newly developed OSHF TFC membranes achieved water flux of 30.2 L m^{-2} h^{-1} and a specific reverse solute flux of 0.13 g L^{-1} using 1M NaCl and DI water as draw and feed solution, respectively. This is a significant improvement on commercial FO membranes. Moreover, this OSHF TFC FO membrane demonstrated higher fouling resistance and better cleaning efficiency against alginate-silica fouling. This membrane also has a strong potential for scale-up for use in larger applications. It also has strong promise for various FO applications such as osmotic membrane bioreactor (OMBR) and fertiliser-drawn OMBR processes.

1. Introduction

Water scarcity is becoming a severe issue in many parts of the world due to the rapid increase in population and the impact of global warming and climate change [1]. A plethora of attempts have been made to develop technologies and water management policies to address this problem, and desalination has proven one of the most reliable options to obtain pure water from the world's unlimited saline water resources and reclaim wastewater [1]. Among the several emerging desalination technologies, forward osmosis (FO) is one of the most promising, with a wide range of applications including seawater desalination [2], wastewater reuse [2, 3], energy production [4, 5], liquid concentration for food processes [6] and fertilizer dilution [7]. The driving force of the FO process is naturally produced by the osmotic pressure difference between draw solution (DS) and feed solution (FS) when they are separated by a semi-permeable membrane [8]. The FO process is considered a low-energy desalination technology compared to other pressure-driven membrane processes, such as ultrafiltration (UF), nanofiltration (NF) and reverse osmosis (RO). Another advantage of the FO process is its low fouling propensity as it requires little or no hydraulic pressure to operate [9]. Investigations of FO's potential have been especially focused on advanced water treatment, including wastewater treatment by aerobic [10] or anaerobic digestion [11] and treatment of backflow wastewater from shale gas exploration [12].

Membranes play a significant role in the forward osmosis (FO) process; hence, membrane design must be carefully considered in order to enhance the overall FO performance. Over the last decade, researchers and industries have considered the development of efficient FO membranes with high water flux and solute rejection for water treatment. A high-performance FO membrane should possess the following properties: (1) a thin selective layer to provide high water permeability and ion selectivity; (2) a porous membrane substrate to alleviate internal

concentration polarization (ICP) [13-15]; and (3) high resistance to membrane fouling [16]. Additionally, FO membranes should also have reasonable mechanical strength to withstand the operating conditions in typical FO processes. However, manufacturing FO membranes with all these desirable properties still remains a challenge. Recent developments of FO membranes have mainly focused on the fabrication of thin-film composite (TFC) membranes composed of a polyamide (PA) selective layer and a support layer (substrate) made of various polymer materials. Sulfonated polymer materials, such as polysulfone (PSf) and polyethersulfone (PES) have been widely employed for FO membrane substrate preparation [8, 13, 15, 17, 18]. TFC FO membranes consist of either flat-sheet or hollow fiber (HF), but HF membranes offer several advantages over the flat-sheet membranes such as a high packing density per module. HF membranes are self-supporting structures, and modulation and scaling-up is easier compared to flat-sheet membranes [19, 20].

However, most HF TFC membranes are designed as inner-selective hollow fibers (ISHF), because they are much easier to manufacture, as discussed later. As the FO process is operated with the selective/active layer of the membrane facing the feed solution (AL-FS), ISHF membranes can be a big problem since the feed solution (FS) containing foulants can cause clogging of the narrow channel of the lumen side (bore side) of the HF substrate, if the feed water is not adequately pre-treated [20-22]. Furthermore, ISHF TFC membranes possess a low surface area per fiber due to their small inner diameter compared to the outer-selective HF (OSHF) TFC membrane. Aquaporin Inside^{TM} recently launched its commercial HF FO membrane modules possessing a thin-film selective layer incorporated with biomimetic aquaporin materials on the bore side of the HF membrane; but the quality of feed water should be critically managed to ensure its stable operation.

On the other hand, the OSHF TFC membrane is more advantageous since the FS can now be located facing the outer surface or shell side of the HF membrane as the active layer is casted on the outer side of the fiber. The OSHF TFC membrane is more preferable over the ISHF TFC membrane because (1) it offers a larger surface area per fiber; (2) lower fouling propensity and easier fouling control on the HF outer surface under AL-FS orientation; and (3) their suitability for application in submerged membrane processes like osmotic membrane bioreactors (OMBR) [23-26]. Equipped with these advantages, the OSHF TFC membrane may be a more suitable candidate for the FO process, especially when it involves treating impaired water/wastewater treatments when a robust pre-treatment system is not in place [27].

Despite its obvious advantages, fabrication of the OSHF TFC membrane is still a challenge, especially the deposition of a defect-free thin PA active layer on the outer surface of a HF membrane substrate. When the fibers are bundled together very close to each other in a module, the fibers touch each other instead of standing freely and independently; and under such conditions, the interfacial polymerization (IP) process should be carefully considered and carried out. This is because when the fibers are touching each other, the effective formation of the PA active layer on the fiber surface becomes a challenge and this can significantly affect the FO performance. In addition, if the fibers are not closely arranged or packed in a module in the IP process, it can significantly reduce the packing density of the HF membrane module, undermining one of the main merits of the HF membrane [26]. Another issue is that although some conventional methods have been used for removing amine solution, such as air purging, roller milling and solvent treatment, they are not effective in the development of OSHF TFC membranes [28]. Nevertheless, Sun et al. first reported the vacuum-assisted IP (VAIP) technique for fabrication of OSHF TFC PRO membranes in 2013 [28]. They demonstrated that the excess MPD solution on the outer

surface of a HF membrane substrate was effectively removed by vacuum suction (800 mbar) to the bore side during the specific time period. Later, more elaborate studies focused on OSHF TFC PRO membranes were conducted by the same group [24, 26]. In particular, Cheng et al. had recently prepared advanced robust OSHF TFC membranes with improved PRO performances [24, 26]. This study also initially benchmarked the concept of VAIP put forward by Sun et al. for developing OSHF TFC FO membranes.

However, contrary to the OSHF TFC membranes for the PRO applications, PA formation by IP process for FO application faces additional challenges [26]. The fiber thickness for FO membranes (70–100 μm) is much smaller and the porosity is much higher compared to PRO membranes (over 200 μm), and hence the FO fiber substrate is much weaker. We expect that this weaker fiber substrate is prone to shrinkage and damage during the VAIP process. To our knowledge, there are only limited studies on the development of the OSHF membrane for FO applications, despite many potential applications such as submerged osmotic membrane bioreactors. Fu et al. and Xia et al. reported a dual-layered HF membrane for PRO processes to generate osmotic power [29, 30]. The outer-selective layer of the HF was composed of polybenzimidazole (PBI) incorporated with polyhedral oligomeric silsesquioxane (POSS), while the inner layer was composed of PAN. This dual-layered membrane exhibited a maximum water flux of 31.4 L m^{-2} h^{-1} and a reverse solute flux (RSF) of 30 g m^{-2} h^{-1} using 2 M $MgCl_2$ under AL-DS of membrane orientation. However, its application for the FO process (AL-FS) has not been tested using NaCl as DS, although its PRO performance using 1 M NaCl DS with DI water as FS reported only 2.7 W m^{-2} of power density, which is much lower than those reported in the literatures The specific RSF (SRSF) of 0.96 g L^{-1} using $MgCl_2$ for this dual-layered PRO membrane indicates that the SRSF of NaCl DS will be significantly higher, which can be highly

problematic for the FO applications, although SRSF is not an issue with the PRO application. Besides, these membrane fabrications require several different types of membrane materials, and the fabrication techniques are currently too complex for commercial scalability.

In this study, we report a successful design and manufacture of OSHF TFC membranes for FO applications, using PES as a membrane substrate and slightly modifying and optimizing the approaches reported in the literature for both fiber manufacture and the IP process. Firstly, the HF spinning parameters were optimized to obtain a membrane substrate with the desired outer surface and inner morphology suitable for subsequent selective PA layer formation. The fibers were then arranged at adequate gaps inside the module to avoid attaching with each other during the IP process. The VAIP approach reported elsewhere [23, 28, 31] was slightly modified for the manufacture of a high-performing OSHF TFC membrane while avoiding shrinkage and membrane substrate damage. All the manufactured OSHF TFC membranes were then characterized, and their FO performances were compared with the commercial FO membranes. In addition, fouling and cleaning tests using alginate and colloidal silica as model foulants were conducted for assessing the fouling potential of OSHF membranes.

To the best of our knowledge, this is the first study on the successful preparation of OSHF TFC FO membranes using a modified VAIP technique. This study also offers insights into the potential scalability of the approaches adopted for the development of OSHF TFC FO membranes.

2. Materials and methods

2.1 Materials and chemicals

Polyethersulfone (PES, Veradel® 3000P, Solvay) within the molecule range of 62,000–64,000 g/mol was dissolved in 1-methyl-2-pyrrolidone (NMP, Merck) for polymer dope preparation to be used in the manufacture of HF substrates. Polyethylene glycol or PEG 400 (PEG 400, M_w = 400 g mol^{-1}, Sigma-Aldrich) was added to the polymer dope as a pore former. 1, 2-phenylenediamine (MPD, 99%) and trimesoyl chloride (TMC, 98%) from Sigma-Aldrich were used for PA selective layer formation on the HF PES substrates via IP reactions. N-hexane (Merck, USA, 99%) was used as the solvent for TMC. Sodium chloride (NaCl, Chem Supply) solution was used as DS for FO performance tests with deionized (DI) water (Milli-Q, Millipore, resistivity 18 MΩ/cm) was used as FS. Glycerol aqueous solution at 50 wt.% was used for the post-treatment of membrane substrates in order to retain their structure. PEG (Sigma-Aldrich) in the molecule range of 6,000–100,000g mol^{-1} and polyethylene oxide (PEO) (Sigma-Aldrich) in the molecule range of 200,000g mol^{-1} were used to determine the pore size distribution of HF membrane substrates. Colloidal silica (100 nm, ST-ZL, Nissan chemical) and sodium alginate (Sigma-Aldrich) were used as model foulants in FS for fouling tests. The commercial flat-sheet (Toray Chemical Korea, Republic of Korea) and ISHF (Aquaporin Inside™, Denmark) TFC FO membranes were obtained from the spiral-wound FO module and the case-housing module (HFFO2) of Aquaporin Inside™, respectively. The commercial FO membranes are denoted as CFS for the Toray flat-sheet (TFC) membrane and CHF for the aquaporin-based biomimetic ISHF thin-film nanocomposite (TFN) membrane.

2.2 Preparation of hollow fiber membrane substrates

A typical dry-jet wet spinning method was applied for preparation of the HF membrane substrates. For the preparation of the polymer dope solution for the membrane substrate, dried PES powder and PEG400 at a fixed amount were mixed with NMP at 60°C for 12 hours using a magnetic stirrer. The addition of hydrophilic non-solvent PEG into the polymer solutions can produce a sponge-like porous morphology for enhancing pore formation and interconnection [24]. The dope solution was then pre-filtered using the 85μm PET mesh (07-85/46, SEFAR) to eliminate impurities. Subsequently, it was loaded into the syringe pump (Model 500D, Teledyne ISCO) and degassed overnight. Dope solution was then pumped into the double spinneret nozzle together with the bore fluid. Specific spinning conditions – including the compositions and flowrate of dope, and bore solutions and take-up speed – were set prior to the dry-jet wet spinning for membrane preparation. These parameters were then adjusted to alter the dimension and morphology of the membrane substrates. In this study, the air-gap distance was carefully manipulated in the range of 2–8 cm to modify the outer surface morphology of the membrane substrates [32, 33]. Figure 1 depicts the schematic diagram for OSHF membrane substrates preparation as a function of the air-gap distance. Detailed spinning conditions of all membrane substrates are presented in Table 1. The HF substrates molded by the nozzle at various air-gap distances were immediately immersed into the coagulation bath to initiate the phase inversion process. The solidified substrates were then rolled up at a specific tension using a roller for straightening the produced fibers. Nascent HF substrates were then stored in DI water for 24 hours to remove the residual solvent and PEG 400 from the samples. The substrates were subsequently immersed in the aqueous glycerol solution

(50 wt.%) for two days. The substrates were then dried in the atmosphere to minimize the collapse of their pore structures in open-air storage.

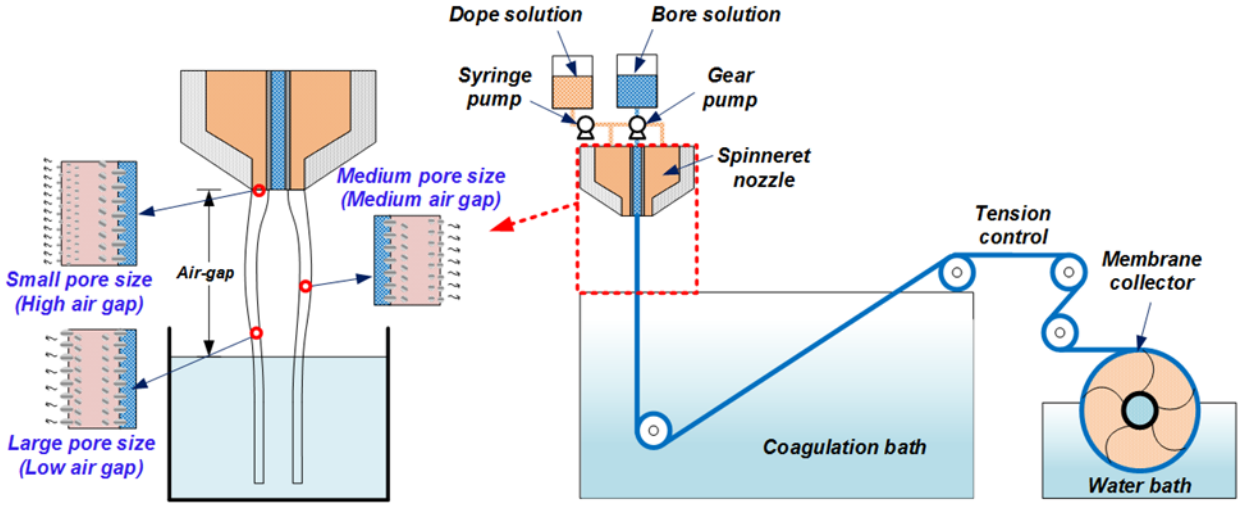

Figure 1. Schematic diagram of HF PES membrane substrate preparation as a function of air-gap distance to manipulate its pore size.

202 **Table 1.** Spinning parameters of HF PES membrane substrates

Membranes	Spinning parameters							Spinneret
	Polymer composition (wt. %)	Dope fluid flowrate (ml/min)	Bore fluid composition (wt. %)	Bore fluid flowrate (ml/min)	Air gap (cm)	Take-up speed (m/min)	External coagulant	ID* / OD* (μm)
HF-1	PES/PEG400/NMP: 16.5/5/78.5	1.8	NMP/DI water: 20/80	3	8	0.74	Tap water	400/1,200
HF-2					6	0.61		
HF-3					2	0.48		

203 * ID: Inner diameter of the spinneret, OD: Outer diameter of the spinneret.

To prepare HF modules, the membrane fibers were carefully spaced in the modules with a specific gap of 0.3 cm in between to avoid the fibers from attaching to each other during the IP process. The module column specially designed for this study was used along with a typical epoxy resin. The effective surface area of the membrane fibers in the module was in the range of 6.5 cm^2 for small-scaled membrane modules and 22.8 cm^2 for larger-scaled membrane modules. Both ends of the modules were capped by cured epoxy resin without deforming the HF membranes' bore holes.

2.3 Preparation of OSHF TFC membranes

The OSHF TFC membranes were prepared by coating a PA selective layer on the outer surface of HF membrane substrates via the IP process using MPD and TMC as aqueous and organic solutions, respectively. Although the VAIP method was initially developed by Sun et al. [28] and Cheng et al. [24] in their studies, the VAIP method applied in this study was slightly modified and is illustrated in Figure 2. The stepwise procedure adopted was as follows:

(1) Membrane substrates, as assembled in the modules, were immersed in DI water for at least 12 hours to remove residual ethylene glycol coated on the membrane structure. (2) The substrates were then dried using a vacuum pump at a pressure of 900 mbar for one minute. (3) Then 2 wt.% MPD aqueous solution mixed with 0.2 wt.% SDS was supplied to the outer surface of the membrane substrates for three minutes. (4) Excess MPD solution was then removed from the shell side of the HF membrane to the bore side using a vacuum pressure of 900 mbar for five minutes. (5) Subsequently, 0.15 wt.% TMC in n-hexane solution was added to the surface of the MPD soaked membrane substrate for one minute in order for the IP reaction to take place. (6) Membrane

modules were then left in the atmosphere for one minute to complete the drying process and they were then cured in an oven at 80°C for ten minutes. (7) Finally, the TFC membrane modules were washed with DI water and stored in DI water at 4°C before being characterized and tested.

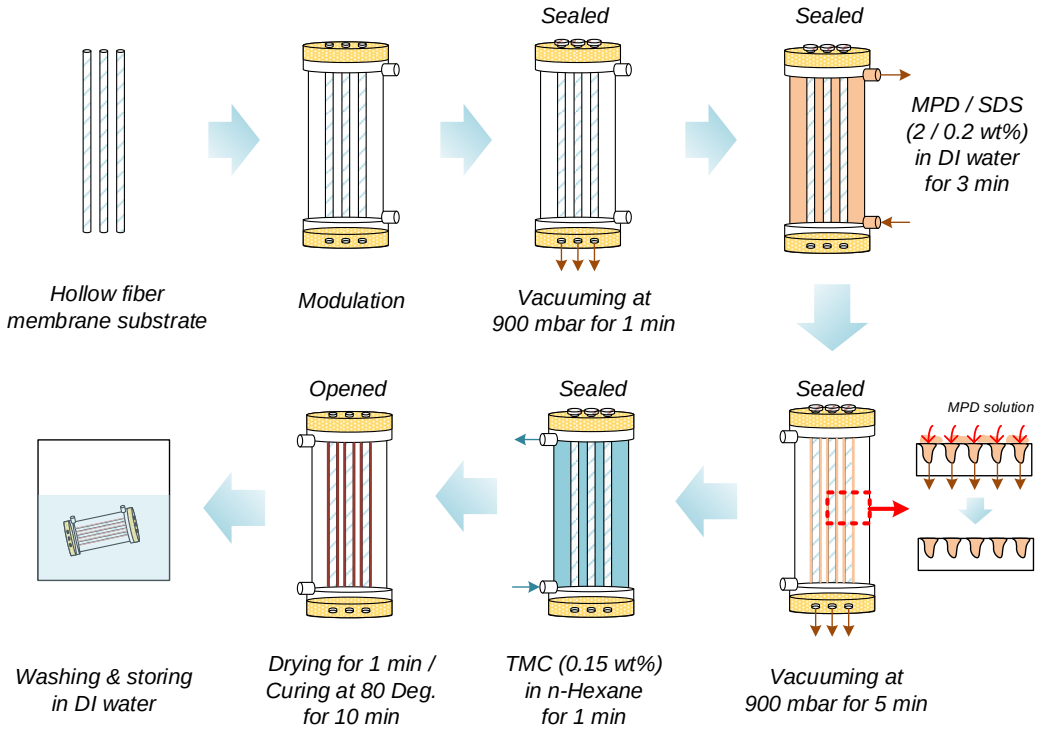

Figure 2. Conceptual illustration of modified interfacial polymerization for OSHF TFC membrane preparation for FO.

2.4 Characterization of membrane substrates

The surface and cross-section morphologies of membrane substrates and the PA selective layer for OSHF TFC membrane were observed by a field emission scanning electron microscope

(FE-SEM, Zeiss Supra 55VP, Carl Zeiss AG) operated at 5 and 10 kV. All membrane samples were coated with gold-palladium using a sputtering coater (EM ACE600, Leica). The membrane substrates were then freeze-fractured for cross-section analysis.

The detailed method for other membrane characterizations such as porosity, pure water permeability (PWP), pore size distribution and MWCO are presented in the supporting information (SI). The membrane characterization was conducted using the same methodology described elsewhere [15, 17].

2.5 Evaluation of OSHF TFC membrane performance

2.5.1 Evaluation of FO performance

The FO performance tests were conducted using the same laboratory-scale FO test unit as described elsewhere [15]. Three kinds of TFC FO membranes – home-made OSHF TFC membranes, commercial ISHF TFC membranes, and flat-sheet commercial TFC membranes – were tested and their performance was compared. The membranes were tested in AL-FS mode using 1 M NaCl solution and DI water as DS and FS, respectively. The detailed method for determining FO performance is shown in the SI.

2.5.2 Determination of intrinsic transport properties of TFC FO membranes

The water permeability coefficient (A), solute permeability coefficient (B), and structural parameter (S) of the OSHF TFC membranes were examined using the 4-stage prediction model

developed by Tiraferri et al. [34]. The averaged values of water flux and reverse solute flux of the membranes measured in various DS concentrations from 0.5 to 2 M were applied to the model calculation. Previous FO studies applied the model prediction, and the detailed information of the model prediction is described elsewhere [34].

2.6 Evaluation of fouling potential on OSHF TFC FO membranes

In order to evaluate the fouling mitigation potential of OSHF TFC membranes, a model aqueous solution containing a 100 nm sized colloidal silica and sodium alginate at 200 mg/L each was used as FS. In addition, a flat-sheet commercial FO membrane was used in the fouling tests as a control sample. Prior to conducting the fouling tests, baseline tests were carried out for 30 minutes with 1 M NaCl solution as a DS, and DI water as a FS. The foulant-spiked solution was then supplied as feed stream while 1 M NaCl solution was used as DS, and both the solutions were continuously circulated in a batch mode of operations. The first cycle was operated with a cross-flow velocity of 10.4 cm for three hours in order to determine the fouling potential. Hydraulic washing was immediately adopted as a physical cleaning strategy using DI water in the feed stream for one hour in order to evaluate the flux decline caused by foulants at the initial stage, and also to determine the flux recovery achieved by physical washing. A cross-flow velocity of 31.2 cm/s was adopted during physical cleaning for both flat-sheet and HF membrane samples, which is three times higher than the velocity used during fouling tests. After the physical cleaning, long-term fouling tests (over ten hours) were conducted immediately using fresh model foulant as FS.

3. Results and discussion

3.1 Characteristics of hollow fiber membrane substrates

Table 2 Intrinsic properties of the OSHF membrane substrates.

	HF-1	HF-2	HF-3
Outer diameter (OD)/ Inner diameter (ID) (μm)	764/643	824/690	975/823
Thickness (μm)	60.5	65.6	77.5
Porosity (%)	69.6±0.6	72.7±0.3	74.1±0.3
Mean pore diameter (nm)	8.0	7.6	13.6
MWCO (kDa)	88.0	85.1	156.9

Table 2 presents the intrinsic properties of OSHF membrane substrates (HF-1, HF-2 and HF-3) including the dimensions, porosity, MWCO, mean pore size and pure water permeability (PWP). The results indicate that the diameter and porosity of the membrane substrates were affected by the air-gap distance used during the fiber spinning. At the lowest air-gap distance of 2 cm, the membrane substrate (HF-3) showed the largest fiber outer/inner diameter (OD/ID: 975/823 μm) and the highest porosity (74.1%) compared to other samples, because of low elongation stress under the fast exchange speed of solvent and non-solvent induced by the external coagulant [33]. However, the fiber diameters and porosities of membrane substrates decreased at a higher air-gap distance of over 6 cm (HF-1 and HF-2) compared to HF-3. These results imply that the overall structure of the membrane substrates shrank and densified with a sponge-like structure because of a greater molecular orientation and chain package by the high gravity induced elongation stress on the fibers in the air-gap region, which may reduce the surface pore size, membrane porosity and free volume of the membrane substrates [33, 35, 36]. Similarly, the mean pore size of HF-3 at 13.6

nm was two times higher than those of HF-1 at 8.0 nm and HF-2 at 7.6 nm. In addition, the MWCO increased from around 87 kDa for HF-1 and HF-2 to 156.9 kDa for HF-3. Moreover, as presented in Figure 3, HF-1 and HF-2 showed almost the same pore sizes with a sharper and narrower size distribution compared to HF-3. Therefore, high air-gap distances of over 6 cm produce membrane substrates with a smaller diameter that have a denser and less porous structure with low and constant pore sizes.

The PWP of the membrane substrates also followed the same trend as their mean pore size and porosity (Figure 3b). Specifically, the PWP of HF-1 and HF-2 were 114.8 and 136.9 $Lm^{-2}h^{-1}bar^{-1}$ respectively, which then drastically increased to 213.9 $Lm^{-2}h^{-1}bar^{-1}$ when the air-gap distance was reduced from 6 cm to 2 cm. The PWP trend correlates well with the pore size and porosity of the membrane substrates produced at different air-gap distances. The PWP depends on the pore size and porosity according to the Hagen-Poiseuille pore flow model [14].

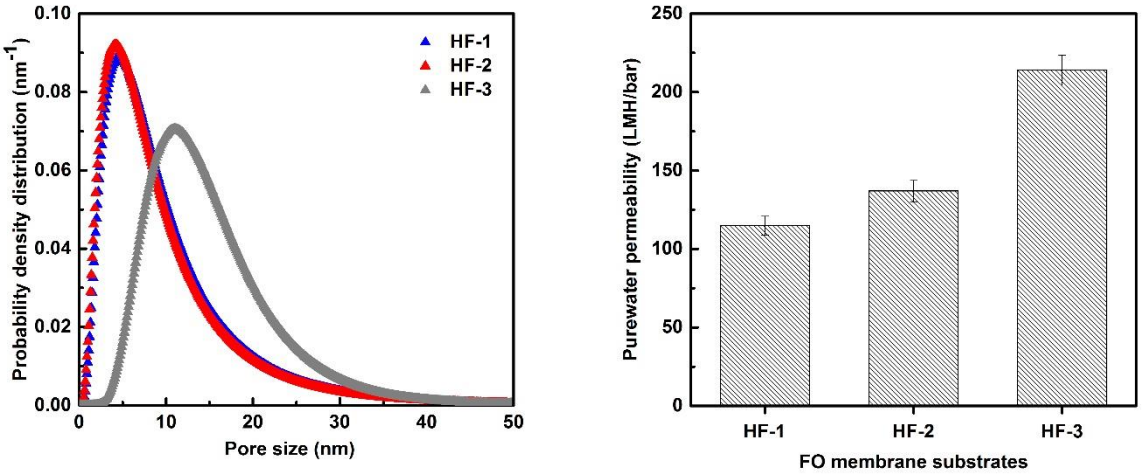

(a) (b)

Figure 3. (a) Pore size distributions and (b) pure water permeability (PWP) of OSHF membrane substrates (HF-1, HF-2 and HF-3) according to various air-gap distances.

The SEM images of the inner surface, cross-section and the outer surface of the membrane substrates are shown in Figure 4. The inner and outer surfaces of all three membrane substrates appear dense and smooth. The morphological differences between the three membranes caused by the air-gap distance cannot be distinguished due to their small pore sizes (less than 10 nm) by the SEM analysis. However, the cross-sectional images of the membrane substrates clearly show the differences in their structural morphology. As expected, the HF-1 substrate exhibited a dense structure with the least number of finger-like voids formed on the inner and outer surfaces. The HF-2 substrate showed larger and more finger-like voids compared to HF-1, while HF-3 had the largest number of finger-like voids with a highly porous structure. These results are also supported by the thickness of membrane substrates as shown in Table 2.

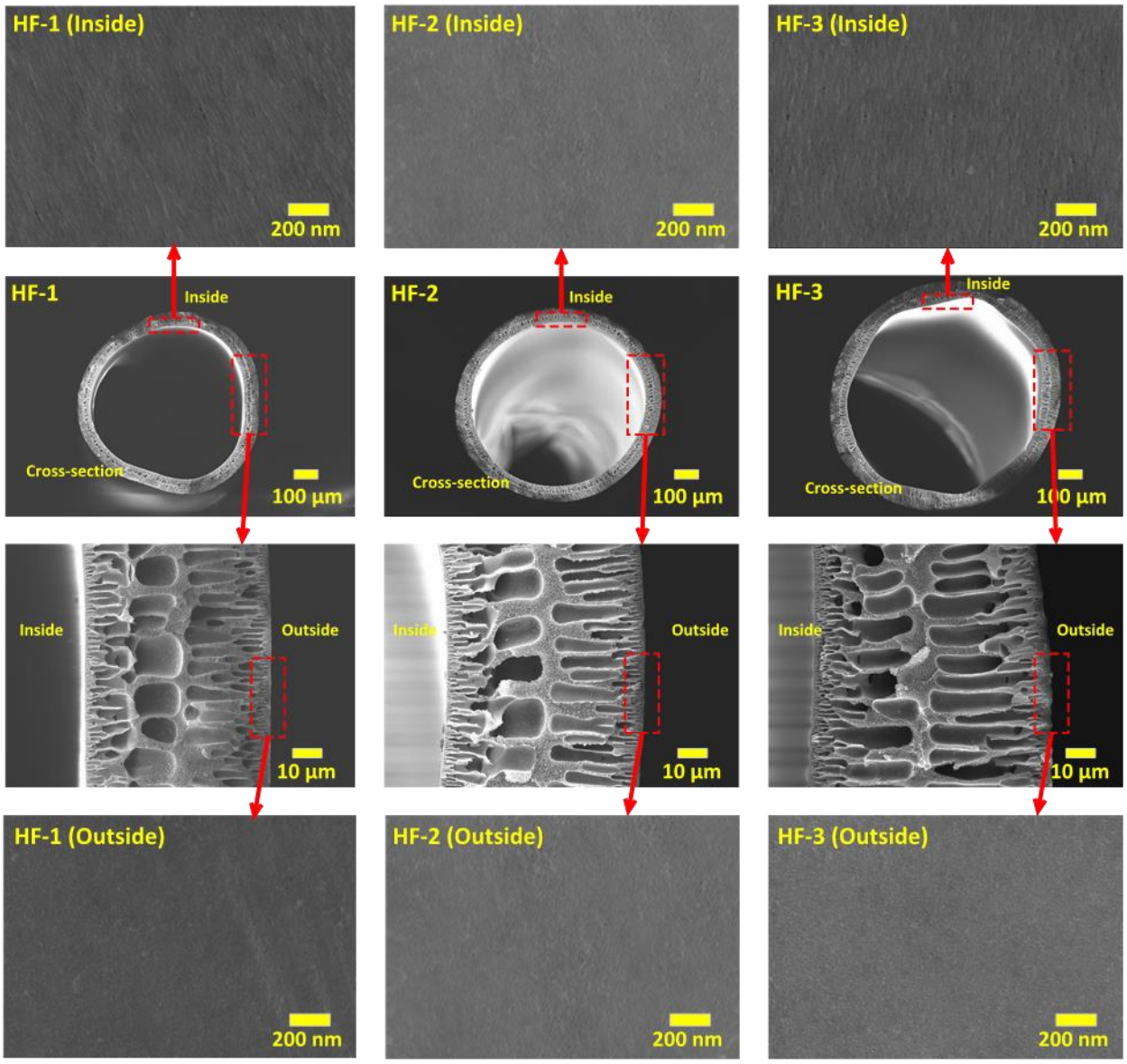

321

322 **Figure 4.** SEM images (inside, outside and cross-section) of hollow fiber membrane substrates

323 (HF-1, HF-2 and HF-3)

324

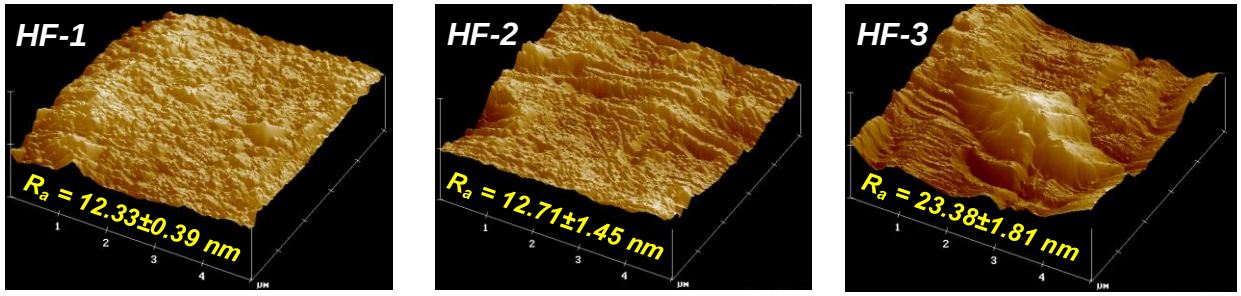

Figure 5 AFM images and average surface roughness (R_a) of OSHF membrane substrates (HF-1, HF-2 and HF-3).

The topographic images of the OSHF membrane substrates presented in Figure 5 show that altering the air-gap distance influenced the outer surface roughness of the membrane. At the shortest air-gap distance, the outer surface of HF-3 demonstrated large nodules and valley-like structures with an average surface roughness of 23.4 nm; whereas HF-1 and HF-2, which had longer air-gap distances, had small nodules with flat and smooth surfaces with an average surface roughness of 12.3 nm and 12.7 nm, respectively . The rough surface of HF-3 may likely prevent the formation of defect-free PA selective layers and hence could negatively affect the FO performance.

3.2 Characteristics and performance of outer-selective hollow fiber (OSHF) TFC membranes

Several studies found that the morphology of the PA active layer strongly depends on the pore structure and chemistry of the skin surface of the membrane substrates (e.g., size and length of pores, porosity, surface roughness, hydrophilicity and reactivity with core chemicals for IP such as MPD and TMC) [24, 37, 38]. In particular, the surface pore size of a membrane substrate can

significantly influence the integrity and morphology of PA selective layer because small and well-dispersed pores can strongly hold a soaked MPD solution within the pores due to the existence of strong surface tension [37]. Consequently, the MPD solution within the surface pores can uniformly diffuse into the TMC solution during the IP process, and it results in the formation of a smooth and thin PA selective layer on the membrane substrate [24]. If the surface pores are large and not well-dispersed, the MPD solution cannot occupy the pores uniformly and will either penetrate inside the pores or will be removed by air-blowing due to the weak surface tension, which will cause rough and defective PA layer formation.

Several studies reported that the pore structure of membrane substrates should be less than 300 kDa MWCO for the formation of a PA selective layer under the typical IP process [37, 39]. In a typical IP process, the MPD solution immediately deposits into the surface pores of the membrane substrates. The excess MPD solution on the membrane substrate is then removed by blowing or purging air onto its surface. However, the excess MPD solution in the VAIP process is mainly sucked from the outer surface towards the bore side using the vacuum-assisted technique. Therefore, the capillary force between the MPD solution and surface pores under the VAIP process should be much stronger than that under the typical IP process. Otherwise, the MPD solution occupied within the large pores with weak capillary force would be mostly removed under the vacuum, which will reduce the integrity of the PA layer. In addition, excess MPD solution in small pores cannot be removed well at relatively low vacuum pressure, as most of the sucked-out air would penetrate via large pores due to their weak capillary forces. The heterogeneous occupation of the MPD solution can lead to the aggregation of the PA layer due to the rapid migration of MPD molecules, which increases the flow turbulence and increases the contact area for the IP reaction

[24]. The hypothesis for the mechanism of PA selective layer formation via VAIP based on the surface pore size of membrane substrates is illustrated in Figure 6 (a).

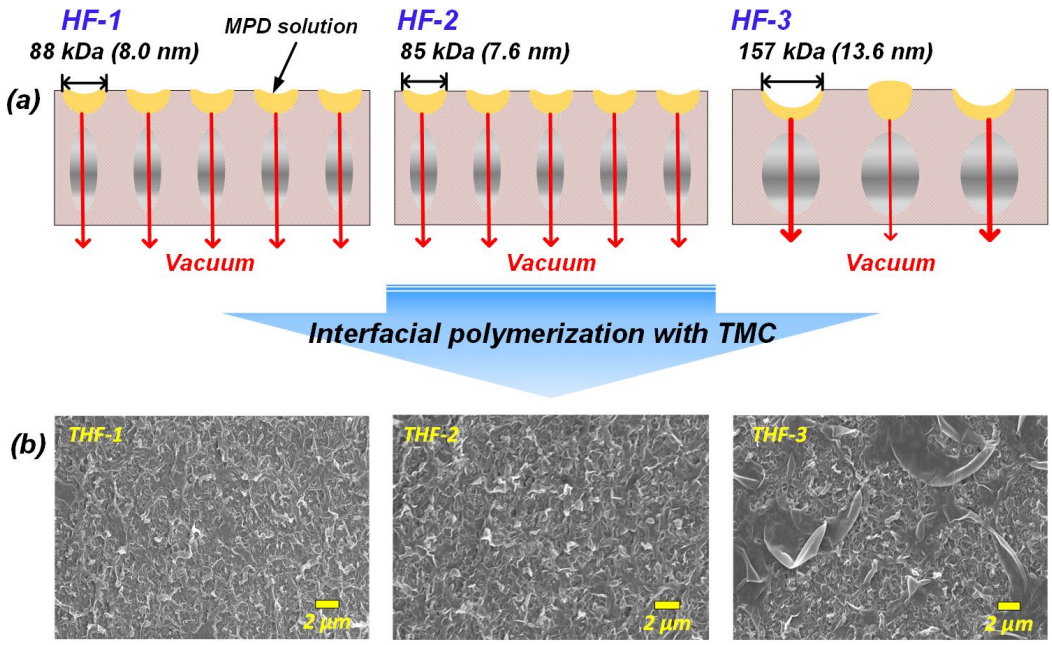

Figure 6 (a) Conceptual illustration of the expected mechanisms of PA selective layer formation via VAIP according to surface pore size of membrane substrates (HF-1, HF-2 and HF-3) and (b) FESEM images of PA selective layers of prepared OSHF TFC hollow fiber membranes (THF-1, THF-2 and THF-3).

Figure 6 (b) shows the morphological images of the PA selective layer formed on the outer surface of HF membrane substrates via the VAIP process. The images of the three TFC membranes (THF-1, THF-2 and THF-3) are visually distinct, especially for THF-3. The selective PA layers of THF-1 and THF-2 possessing smaller pore size substrate are observed to be smoother, thinner and

well formed with relatively small globules. In contrast, the THF-3 membrane with larger pore substrates and varied pore size distribution shows the formation of a relatively rougher and thicker PA layer with large globules on its surface. Rapid migration of MPD molecules, as mentioned earlier, may cause the formation of a defective PA layer on the THF-3 substrate [24, 38]. Based on the SEM images demonstrated in Figure 6b, THF-3 is expected to show relatively poor performances compared to the other two membranes. Based on these results, membrane substrates possessing well-distributed pores with its MWCO less than 88 kDa is more suitable for producing a defect-free PA selective layer via the VAIP process.

The FO performance (water flux and SRSF) tests of the home-made OSHF TFC membranes and commercial flat-sheet TFC FO membranes were conducted using 1M NaCl as DS, and DI water as FS, under AL-FS orientation. As shown in Figure 7, THF-2 achieved the best FO performance compared to other home-made OSHF TFC membranes, demonstrating the highest water flux of 30.2 L m^{-2} h^{-1} and the lowest SRSF value of 0.13 g L^{-1}. The water flux of THF-1 was slightly lower at 25.6 L m^{-2} h^{-1}, and its SRSF was slightly higher at 0.21 g L^{-1}. This is likely because the THF-1 membrane substrate has lower porosity and permeability even though it is thinner than the THF-2 membrane. Although the PA selective layer of both THF-1 and THF-2 were well formed on the membrane substrate due to their favorable surface morphology, THF-1 is likely to have a higher ICP effect because of its lower porosity resulting in lower water flux. The water flux of THF-3 was significantly lower at 20.1 L m^{-2} h^{-1}, and its SRSF was much higher at 0.4 g L^{-1}. The poor selectivity of the THF-3 membrane is likely due to the defective PA active layer formed on its substrate as corroborated by the SEM images in Figure 6. Although the PWP of the THF-3 membrane is higher, the lower FO water flux is likely due to the leaky active layer as a result of defects that reduce the osmotic driving force. The large and heterogeneous surface pores formed

401 on the skin layer of the membrane substrate, and the high level of roughness of the membrane
402 substrate (HF-3) likely caused the poor PA layer formation. Under the similar feed and draw
403 solution conditions, the commercial flat-sheet (CFS) membrane showed an FO water flux of 35.4
404 L m^{-2} h^{-1}, slightly higher than that of THF-2; however, its SRSF of 0.34 g L^{-1} was about 2.5 times
405 higher than that of THF-2. The SRSF is particularly important for most FO applications because
406 it not only loses the draw solutes but also reduces the effective osmotic driving force and can
407 complicate the feed brine management. Although the SRSF of the commercial hollow fiber (CHF)
408 membrane was similar to the THF-2 membrane, the water flux of CHF (14.3 L m^{-2} h^{-1}) was much
409 lower than that of the THF-2 membrane.

410

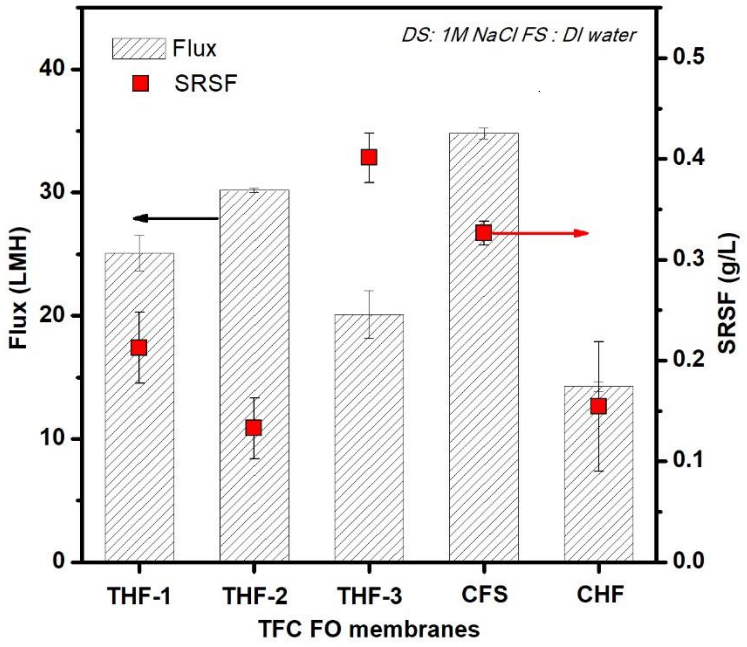

411

412 **Figure 7** FO performance (water flux and specific reverse solute flux) of OSHF TFC membranes
413 (HF-1, 2 and 3), commercial flat-sheet (CFS) and inner-selective hollow fiber (CHF) TFC
414 membranes using 1 M NaCl solution as DS and DI water as FS.

Figure 8 shows the comparative profiles of the water flux and SRSF of the FO membranes at different DS concentrations. The water fluxes of all FO membranes gradually increased when higher concentrated DS was used, which was the expected result due to a higher net osmotic driving force generated by the DS. The THF-2 membrane consistently exhibited the highest water flux and the lowest SRSF among all the OSHF TFC membrane samples tested, confirming the results shown in Figure 7.

The intrinsic transport properties of the HF membranes, such as water permeability coefficient (*A*), solute permeability coefficient (*B*) and structural parameter (*S*) values, which were estimated based on the FO model algorithm by Tiraferri et al., are presented in Table 3 obtained based on the FO data in Figure 8 [34]. Although the mass transfer phenomena of flat-sheet and HF membranes are quite different due to the curvature effect of HF membranes; unlike flat-sheet membranes, Lin suggested that the mass transfer equations for flat-sheet membranes can be applied for estimating the mass transfer under a HF geometry [40]. The *A* and *B* values of the THF-2 membrane were 2.26 L m^{-2} h^{-1} $bar^{-1,}$ and 0.28 L m^{-2} h^{-1} respectively. The intrinsic selectivity (*B/A*) of THF-2 at 0.12 bar was the lowest compared to all the membrane samples evaluated in this study. However, both the *A* (2.45 L m^{-2} h^{-1} bar^{-1}) and *B* (0.77 L m^{-2} h^{-1}) values of THF-3 were higher than those of other membrane samples, probably because of the defective PA selective layer formed for the THF-3 membrane as explained earlier. Although the *A* value of CFS was relatively high, its *B* value was also extremely high compared to those of THF-1 and THF-2 so that its intrinsic selectivity at 0.31 bar was significantly higher than the THF-1 at 0.18 bar and THF-2 at 0.12 bar. Contrary to CFS, the inner-selective CHF membrane showed the lowest *A* and *B* values, because of which its intrinsic selectivity was also observed to be the lowest at 0.11 bar, comparable to that of the THF-2 membrane. Furthermore, the *S* value of 190 μm for THF-2 membrane was

found to be the lowest among all the membrane samples tested, which can be attributed to the high porosity and permeability of the membrane substrate. Due to the significantly higher performances of the THF-2 membrane in terms of water flux and SRSF, it can be concluded that THF-2 is the optimal OSHF TFC membrane manufactured in this study, and also indicates that the HF-2 membrane substrate possessed the most desirable morphological properties for water transport and PA layer formation.

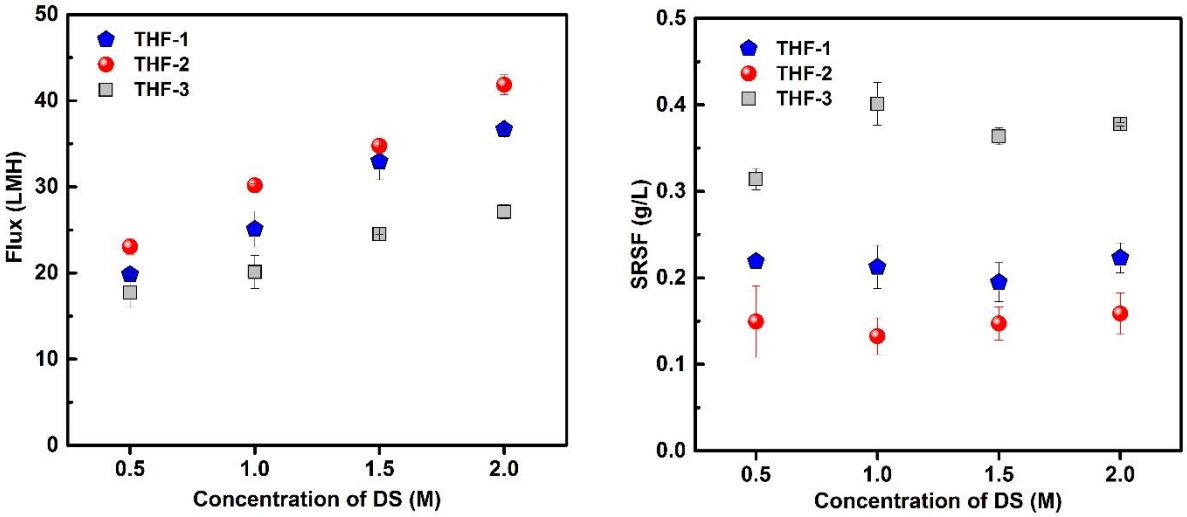

(a) (b)

Figure 8. Water flux (a) and specific reverse solute flux - SRSF (b) of home-made OSHF TFC membranes under different NaCl concentrations from 0.5 to 2 M as DS and DI water as FS.

Table 3. Intrinsic transport properties of newly designed OSHF FO membranes.

FO membranes	*A* ($Lm^{-2}h^{-1}bar^{-1}$)	*B* ($Lm^{-2}h^{-1}$)	*B/A* (bar)	*S* (μm)
THF-1	1.68	0.30	0.18	214
THF-2	2.26	0.28	0.12	190
THF-3	2.45	0.77	0.31	428
CFS	1.63	0.65	0.40	312
CHF	0.71	0.08	0.11	312

3.3 Fouling and cleaning of the flat sheet and hollow fiber TFC membranes under FO operation

The fouling and cleaning tests were conducted for OSHF TFC membrane samples (THF-2, THF-3) and commercial membranes (CFS and CHF) in order to comparatively evaluate their fouling potential and cleaning efficiency. For OSHF TFC membranes, THF-2 and THF-3 were selected as the best and worst sample respectively based on the results of their performance tests. Figure 9 presents the variation in the normalized water flux (J_w/J_0) of the membranes as a function of the operating time (h). The normalized water fluxes of all membranes in Stage 1 began to decline, most likely because of pore blocking. Although the two home-made OSHF membranes showed a rapid initial flux decline similar to other membranes, its flux, nevertheless, gradually stabilized after a certain period of time within Stage 1 at a normalized flux of 0.92 for THF-2 and 0.88 for THF-3. For commercial FO membranes (CFS and CHF), the water fluxes continuously dropped reaching a normalized flux of 0.85 for CFS and 0.91 for CHF after three hours of operation. Although all TFC membranes in this study were not chemically modified, their fouling potential varied quite significantly. The high-flux membrane samples such as THF-2 and CFS cause high fouling potential compared to those of low-flux samples (THF-3 and CHF). In addition, poor ion

selectivity of the membrane samples (THF-3 and CFS) may cause the acceleration of colloidal fouling on the membrane surface due to the electrostatic attraction between penetrated ions and charged foulants [41, 42]. These results, therefore, clearly indicate that the THF-2 membrane sample possesses lower fouling potential among all the membrane samples, even though its water flux was significantly higher.

Subsequently, the hydraulic washing of the fouled membranes was conducted for one hour using DI water as a cleaning agent after the completion of the Stage 1 operation. The cross-flow velocity used for physical cleaning was three times higher than that under the normal FO operation in Stage 1 and Stage 2. The hydraulic washing data for inner-selective CHF membrane could not be presented in Figure 9 as the mechanical strength of the membrane was not adequate to withstand the high flow rate used inside as bore fluid for the hydraulic cleaning. In addition, foulants might also clog the fiber bore increasing the pressure drop. The water flux recovery rates of THF-2 and THF-3 after hydraulic cleaning following its operation in Stage 1 were more than 99%, while it was slightly lower, at 95%, for CFS membrane.

Fouling experiments were then resumed for ten hours in Stage 2 using a new alginate-silica mixture as model foulants. The flux decline trend for THF-2, THF-3 and CFS in Stage 2 were similar to those observed in Stage 1. The highest flux decline was observed for commercial CFS membrane dropping to a nominalized water flux of 0.64 after ten hours. On the other hand, the water flux of THF-2 and THF-3 declined only slightly at first and then gradually stabilized at 0.92 and 0.88 respectively during ten hours of fouling tests. The flux decline rate of THF-2 membrane was lower than that of THF-3 during the fouling test in both Stage 1 and Stage 2. With regard to the performance tests, THF-3 produced lower water flux and higher SRSF compared to the THF-2 TFC membrane, which could be ascribed to the defective PA layer of the THF-3 membrane. The

489 higher flux decline of THF-3 in the fouling test using the silica and alginate might be attributed to
490 membrane's high reverse diffusion of draw solutes, although its initial water flux was lower than
491 that of THF-2. In addition, the large granular morphology of the THF-3 PA layer may also likely
492 accelerate membrane fouling as the particulates can easily deposit on the membrane surface [43].

493 Overall, the THF-2 membrane presented the best fouling resistance and cleaning efficiency
494 during the fouling tests compared to other OSHF and commercial membranes. Based on overall
495 FO performance and fouling test results, it implies that the THF-2 membrane is a promising
496 candidate for FO applications with better performance and fouling resistance compared to
497 commercial FO membranes. Based on the results, we believe that the optimized OSHF FO
498 membrane (THF-2) can be a suitable candidate for the water treatment in a foulant rich
499 environment such as submerged OMBR applications for wastewater treatment using reverse
500 osmosis brine or concentrated fertilizer as DS, where the influent stream or bioreactor with foulants
501 will face the outer-selective layer of the membrane [44, 45]. Nevertheless, it is necessary to further
502 investigate the fouling and application studies of the OSHF FO membranes in the future to better
503 understand and further mitigate the fouling phenomenon.

504

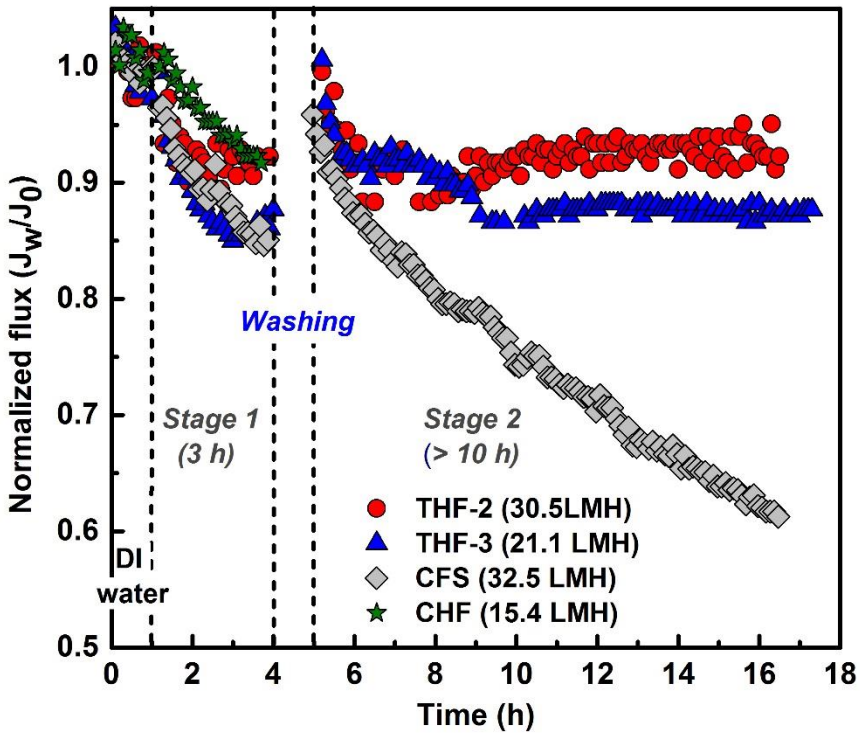

505

506 **Figure 9** Comparison of fouling propensity and cleaning efficiency of OSHF TFC and commercial
507 FO membranes during stabilization, Stage 1 and Stage 2. DI water spiked with sodium alginate
508 (200 mg/L) and colloidal silica (200 mg/L) was used as a feed solution, and 1 M NaCl solution
509 was used as a draw solution. DI water was supplied into the feed stream for physical cleaning. The
510 initial water fluxes of the membrane samples during the stabilization were varied, as shown in the
511 figure. The cross-flow velocity of the feed stream for membrane fouling and cleaning was
512 maintained at 10.4 and 31.2 cm/sec, respectively.

513

514

3.4 Evaluating the scalability of OSHF TFC membrane modules

All the OSHF TFC membrane lab-scale modules used in this study contained only two membrane fibers with a surface area of 6.5 cm^2, which can be a challenge when understanding the scalability of the OSHF TFC membrane modules and their stability during FO operation. In addition, it was important to investigate the feasibility of VAIP technique application to a large-scale module. This is because the VAIP technique requires the vacuum pressure to be applied equally into each module fiber in order to properly remove the excess MPD solution on the outer surface for subsequent PA formation. A number of larger membrane modules, containing eight HFs of THF-2 with a total surface area of 22.8 cm^2, were thus manufactured for further performance tests. The experimental results of the larger-scale modules were compared with those of the small-scale modules (two fibers of THF-2). Figure 10 presents the FO water fluxes and SRSF of slightly scaled-up THF-2 membrane modules. This scaled-up OSHF TFC membrane module exhibited water flux (30.7 L m^{-2} h^{-1}) and SRSF (0.17 g L^{-1}) which were similar to those of small-scaled membrane module (water flux of 30.2 L m^{-2} h^{-1} and SRSF of 0.13 g L^{-1}). These results indicated that the modified VAIP could be suitable for developing the larger-scale FO module with OSHF TFC membrane for commercial-scale operation in the future. The authors did not have the facilities to build and test HF membrane modules larger than the one used in this study. Although hydraulic pressure is not applied in FO processes unlike RO, FO membranes may incur mechanical stress, which may damage the membranes in a module. Therefore, the future work will involve the development of OSHF TFC membranes with high mechanical strength in order to build commercial-scale modules for practical applications.

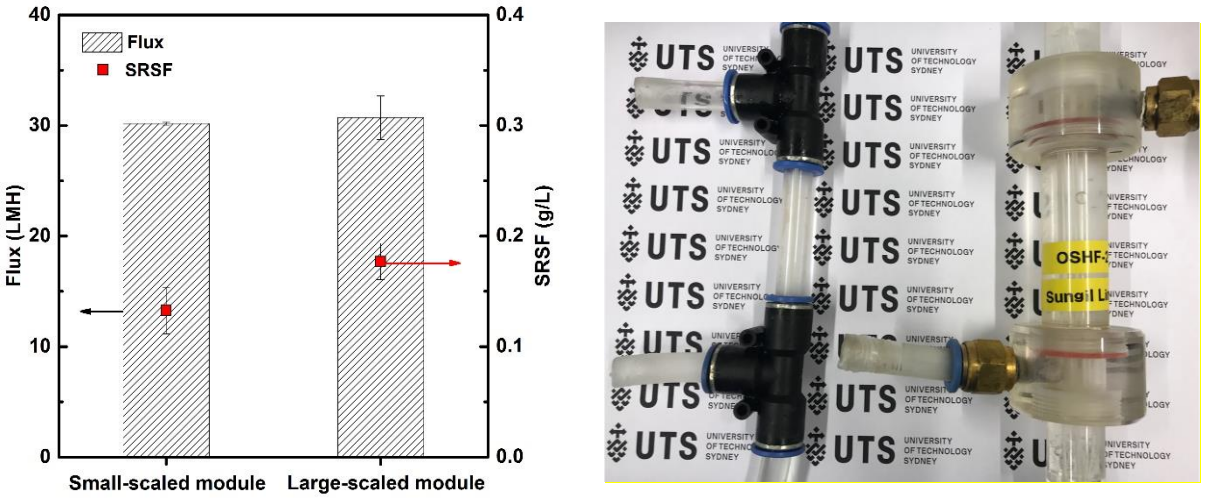

(a) (b)

537

538 **Figure 10.** (a) Water flux and SRSF of small-scale and large-scale THF-2 membrane modules and

539 (b) their real picture (Left: small-scale module, Right: large-scale module) with 1M NaCl as DS

540 and DI water as FS.

541

542

4. Conclusion

A number of novel OSHF TFC FO membranes were successfully developed for FO applications. This study presented a practical approach on how to manufacture the optimum OSHF TFC membranes starting with the design of the outer surface of HF membrane substrates as a function of air-gap distance followed by a modified VAIP technique for PA selective layer formation. This modified approach could successfully develop a defect-free PA layer on the outer surface of the hollow fiber membrane. The best performance OSHF TFC FO membrane fabricated using an air-gap of 6 cm exhibited a water flux of 30.2 L m^{-2} h^{-1} and SRSF of 0.13 g L^{-1} with 1M NaCl and DI water as DS and FS, respectively. Additionally, this membrane demonstrated a high fouling resistance and a higher cleaning efficiency when tested using the silica-alginate spiked solution. The novel OSHF TFC FO membrane is potentially one of the most suitable candidates for newly emerging FO applications such as submerged aerobic or anaerobic OMBR, and a fertilizer-drawn OMBR hybrid system with less concern about low water flux, salinity build-up, membrane fouling and cleaning, as well as membrane modulation. Using the fabrication protocol and guidelines suggested in this study, further modifications such as incorporating a braid into the HF support layer are required to enhance the mechanical strength of the membranes to ensure feasibility in practical applications.

5. Acknowledgement

This research was supported by the Australian Research Council (ARC) Future Fellowship (FT140101208) and by Korea Environment Industry & Technology Institute (KEITI) through Industrial Facilities & Infrastructure Research Program, funded by Korea Ministry of Environment (MOE) (88107).

6. References

[1] M.A. Shannon, P.W. Bohn, M. Elimelech, J.G. Georgiadis, B.J. Mariñas, A.M. Mayes, Science and technology for water purification in the coming decades, Nature, 452 (2008) 301.

[2] R. Valladares Linares, Z. Li, S. Sarp, S.S. Bucs, G. Amy, J.S. Vrouwenvelder, Forward osmosis niches in seawater desalination and wastewater reuse, Water Research, 66 (2014) 122-139.

[3] K. Lutchmiah, A.R.D. Verliefde, K. Roest, L.C. Rietveld, E.R. Cornelissen, Forward osmosis for application in wastewater treatment: A review, Water Research, 58 (2014) 179-197.

[4] G. Han, S. Zhang, X. Li, T.-S. Chung, Progress in pressure retarded osmosis (PRO) membranes for osmotic power generation, Progress in Polymer Science, 51 (2015) 1-27.

[5] S. Lim, M.J. Park, S. Phuntsho, A. Mai-Prochnow, A.B. Murphy, D. Seo, H. Shon, Dual-layered nanocomposite membrane incorporating graphene oxide and halloysite nanotube for high osmotic power density and fouling resistance, Journal of Membrane Science, 564 (2018) 382-393.

[6] B.S. Chanukya, N.K. Rastogi, Ultrasound assisted forward osmosis concentration of fruit juice and natural colorant, Ultrasonics Sonochemistry, 34 (2017) 426-435.

582 [7] S. Phuntsho, H.K. Shon, S. Hong, S. Lee, S. Vigneswaran, A novel low energy fertilizer driven
583 forward osmosis desalination for direct fertigation: Evaluating the performance of fertilizer draw
584 solutions, Journal of Membrane Science, 375 (2011) 172-181.
585 [8] Y. Zhao, X. Wang, Y. Ren, D. Pei, Mesh-Embedded Polysulfone/Sulfonated Polysulfone
586 Supported Thin Film Composite Membranes for Forward Osmosis, ACS Applied Materials &
587 Interfaces, 10 (2018) 2918-2928.
588 [9] N. Akther, A. Sodiq, A. Giwa, S. Daer, H.A. Arafat, S.W. Hasan, Recent advancements in
589 forward osmosis desalination: A review, Chemical Engineering Journal, 281 (2015) 502-522.
590 [10] R.W. Holloway, J. Regnery, L.D. Nghiem, T.Y. Cath, Removal of Trace Organic Chemicals
591 and Performance of a Novel Hybrid Ultrafiltration-Osmotic Membrane Bioreactor, Environmental
592 Science & Technology, 48 (2014) 10859-10868.
593 [11] A. Achilli, T.Y. Cath, E.A. Marchand, A.E. Childress, The forward osmosis membrane
594 bioreactor: A low fouling alternative to MBR processes, Desalination, 239 (2009) 10-21.
595 [12] D.L. Shaffer, L.H. Arias Chavez, M. Ben-Sasson, S. Romero-Vargas Castrillón, N.Y. Yip, M.
596 Elimelech, Desalination and Reuse of High-Salinity Shale Gas Produced Water: Drivers,
597 Technologies, and Future Directions, Environmental Science & Technology, 47 (2013) 9569-9583.
598 [13] P. Xiao, L.D. Nghiem, Y. Yin, X.-M. Li, M. Zhang, G. Chen, J. Song, T. He, A sacrificial-
599 layer approach to fabricate polysulfone support for forward osmosis thin-film composite
600 membranes with reduced internal concentration polarisation, Journal of Membrane Science, 481
601 (2015) 106-114.
602 [14] X. Liu, H.Y. Ng, Double-blade casting technique for optimizing substrate membrane in thin-
603 film composite forward osmosis membrane fabrication, Journal of Membrane Science, 469 (2014)
604 12-126.

[15] S. Lim, M.J. Park, S. Phuntsho, L.D. Tijing, G.M. Nisola, W.-G. Shim, W.-J. Chung, H.K. Shon, Dual-layered nanocomposite substrate membrane based on polysulfone/graphene oxide for mitigating internal concentration polarization in forward osmosis, Polymer, 110 (2017) 36-48.

[16] A. Tiraferri, Y. Kang, E.P. Giannelis, M. Elimelech, Highly Hydrophilic Thin-Film Composite Forward Osmosis Membranes Functionalized with Surface-Tailored Nanoparticles, ACS Applied Materials & Interfaces, 4 (2012) 5044-5053.

[17] N. Widjojo, T.-S. Chung, M. Weber, C. Maletzko, V. Warzelhan, The role of sulphonated polymer and macrovoid-free structure in the support layer for thin-film composite (TFC) forward osmosis (FO) membranes, Journal of Membrane Science, 383 (2011) 214-223.

[18] N. Akther, S. Lim, V.H. Tran, S. Phuntsho, Y. Yang, T.-H. Bae, N. Ghaffour, H.K. Shon, The effect of Schiff base network on the separation performance of thin film nanocomposite forward osmosis membranes, Separation and Purification Technology, 217 (2019) 284-293.

[19] J. Ren, M.R. Chowdhury, J. Qi, L. Xia, B.D. Huey, J.R. McCutcheon, Relating osmotic performance of thin film composite hollow fiber membranes to support layer surface pore size, Journal of Membrane Science, 540 (2017) 344-353.

[20] P. Zhong, X. Fu, T.-S. Chung, M. Weber, C. Maletzko, Development of Thin-Film Composite forward Osmosis Hollow Fiber Membranes Using Direct Sulfonated Polyphenylenesulfone (sPPSU) as Membrane Substrates, Environmental Science & Technology, 47 (2013) 7430-7436.

[21] R.C. Ong, T.-S. Chung, J.S. de Wit, B.J. Helmer, Novel cellulose ester substrates for high performance flat-sheet thin-film composite (TFC) forward osmosis (FO) membranes, Journal of Membrane Science, 473 (2015) 63-71.

[22] J. Ren, J.R. McCutcheon, Making Thin Film Composite Hollow Fiber Forward Osmosis Membranes at the Module Scale Using Commercial Ultrafiltration Membranes, Industrial & Engineering Chemistry Research, 56 (2017) 4074-4082.

[23] N.L. Le, N.M.S. Bettahalli, S.P. Nunes, T.-S. Chung, Outer-selective thin film composite (TFC) hollow fiber membranes for osmotic power generation, Journal of Membrane Science, 505 (2016) 157-166.

[24] Z.L. Cheng, X. Li, Y.D. Liu, T.-S. Chung, Robust outer-selective thin-film composite polyethersulfone hollow fiber membranes with low reverse salt flux for renewable salinity-gradient energy generation, Journal of Membrane Science, 506 (2016) 119-129.

[25] J. Ren, J.R. McCutcheon, Polyacrylonitrile supported thin film composite hollow fiber membranes for forward osmosis, Desalination, 372 (2015) 67-74.

[26] Z.L. Cheng, X. Li, Y. Feng, C.F. Wan, T.-S. Chung, Tuning water content in polymer dopes to boost the performance of outer-selective thin-film composite (TFC) hollow fiber membranes for osmotic power generation, Journal of Membrane Science, 524 (2017) 97-107.

[27] V.H. Tran, S. Lim, D.S. Han, N. Pathak, N. Akther, S. Phuntsho, H. Park, H.K. Shon, Efficient fouling control using outer-selective hollow fiber thin-film composite membranes for osmotic membrane bioreactor applications, Bioresource Technology, 282 (2019) 9-17.

[28] S.-P. Sun, T.-S. Chung, Outer-Selective Pressure-Retarded Osmosis Hollow Fiber Membranes from Vacuum-Assisted Interfacial Polymerization for Osmotic Power Generation, Environmental Science & Technology, 47 (2013) 13167-13174.

[29] Q.-C. Xia, M.-L. Liu, X.-L. Cao, Y. Wang, W. Xing, S.-P. Sun, Structure design and applications of dual-layer polymeric membranes, Journal of Membrane Science, 562 (2018) 85-111.

649 [30] F.-J. Fu, S. Zhang, S.-P. Sun, K.-Y. Wang, T.-S. Chung, POSS-containing delamination-free
650 dual-layer hollow fiber membranes for forward osmosis and osmotic power generation, Journal of
651 Membrane Science, 443 (2013) 144-155.
652 [31] Z.L. Cheng, X. Li, Y.D. Liu, T.-S. Chung, Robust outer-selective thin-film composite
653 polyethersulfone hollow fiber membranes with low reverse salt flux for renewable salinity-
654 gradient energy generation, Journal of Membrane Science, 506 (2016) 119-129.
655 [32] N. Noor, J. Koll, C. Abetz, H. Notzke, V. Abetz, Continuous Production of Macroporous
656 Films: an Alternative to Breath Figure Assembly, Scientific Reports, 7 (2017) 8050.
657 [33] M. Khayet, The effects of air gap length on the internal and external morphology of hollow
658 fiber membranes, Chemical Engineering Science, 58 (2003) 3091-3104.
659 [34] A. Tiraferri, N.Y. Yip, A.P. Straub, S. Romero-Vargas Castrillon, M. Elimelech, A method
660 for the simultaneous determination of transport and structural parameters of forward osmosis
661 membranes, Journal of Membrane Science, 444 (2013) 523-538.
662 [35] T.-S. Chung, X. Hu, Effect of air-gap distance on the morphology and thermal properties of
663 polyethersulfone hollow fibers, Journal of Applied Polymer Science, 66 (1997) 1067-1077.
664 [36] J.-J. Qin, J. Gu, T.-S. Chung, Effect of wet and dry-jet wet spinning on the shear-induced
665 orientation during the formation of ultrafiltration hollow fiber membranes, Journal of Membrane
666 Science, 182 (2001) 57-75.
667 [37] L. Shi, S.R. Chou, R. Wang, W.X. Fang, C.Y. Tang, A.G. Fane, Effect of substrate structure
668 on the performance of thin-film composite forward osmosis hollow fiber membranes, Journal of
669 Membrane Science, 382 (2011) 116-123.

[38] A.K. Ghosh, E.M.V. Hoek, Impacts of support membrane structure and chemistry on polyamide-polysulfone interfacial composite membranes, Journal of Membrane Science, 336 (2009) 140-148.

[39] Y. Wang, T. Xu, Anchoring hydrophilic polymer in substrate: An easy approach for improving the performance of TFC FO membrane, Journal of Membrane Science, 476 (2015) 330-339.

[40] S. Lin, Mass transfer in forward osmosis with hollow fiber membranes, Journal of Membrane Science, 514 (2016) 176-185.

[41] G. Han, J. Zhou, C. Wan, T. Yang, T.-S. Chung, Investigations of inorganic and organic fouling behaviors, antifouling and cleaning strategies for pressure retarded osmosis (PRO) membrane using seawater desalination brine and wastewater, Water Research, 103 (2016) 264-275.

[42] S.C. Chen, C.F. Wan, T.-S. Chung, Enhanced fouling by inorganic and organic foulants on pressure retarded osmosis (PRO) hollow fiber membranes under high pressures, Journal of Membrane Science, 479 (2015) 190-203.

[43] M. Elimelech, Z. Xiaohua, A.E. Childress, H. Seungkwan, Role of membrane surface morphology in colloidal fouling of cellulose acetate and composite aromatic polyamide reverse osmosis membranes, Journal of Membrane Science, 127 (1997) 101-109.

[44] N. Pathak, L. Chekli, J. Wang, Y. Kim, S. Phuntsho, S. Li, N. Ghaffour, T. Leiknes, H. Shon, Performance of a novel baffled osmotic membrane bioreactor-microfiltration hybrid system under continuous operation for simultaneous nutrient removal and mitigation of brine discharge, Bioresource Technology, 240 (2017) 50-58.

692 [45] Y. Kim, L. Chekli, W.-G. Shim, S. Phuntsho, S. Li, N. Ghaffour, T. Leiknes, H.K. Shon,
693 Selection of suitable fertilizer draw solute for a novel fertilizer-drawn forward osmosis–anaerobic
694 membrane bioreactor hybrid system, Bioresource Technology, 210 (2016) 26-34.
695